Characterization of the Diffusion Coefficient of Blood

Carsten Funck,[1] Frederik Bernd Laun,[1,2] and Andreas Wetscherek[1,3]*

Purpose: To characterize the diffusion coefficient of human blood for accurate results in intravoxel incoherent motion imaging.
Methods: Diffusion-weighted MRI of blood samples from 10 healthy volunteers was acquired with a single-shot echo-planar-imaging sequence at body temperature. Effects of gradient profile (monopolar or flow-compensated), diffusion time (40–100 ms), and echo time (60–200 ms) were investigated.
Results: Although measured apparent diffusion coefficients of blood were larger for flow-compensated than for monopolar gradients, no dependence of the apparent diffusion coefficient on the diffusion time was found. Large differences between individual samples were observed, with results ranging from 1.26 to 1.66 μm^2/ms for flow-compensated and 0.94 to 1.52 μm^2/ms for monopolar gradients. Statistical analysis indicates correlations of the flow-compensated apparent diffusion coefficient with hematocrit ($P = 0.007$) and hemoglobin ($P = 0.017$), but not with mean corpuscular volume ($P = 0.64$). Results of Monte-Carlo simulations support the experimental observations.
Conclusions: Measured blood apparent diffusion coefficient values depend on hematocrit/hemoglobin concentration and applied gradient profile due to non-Gaussian diffusion. Because in vivo measurement is delicate, an estimation based on blood count results could be an alternative. For intravoxel incoherent motion modeling, the use of a blood self-diffusion constant $D_b = 1.54 \pm 0.12\ \mu m^2$/ms for flow-compensated and $D_b = 1.30 \pm 0.18\ \mu m^2$/ms for monopolar encoding is suggested. **Magn Reson Med 000:000–000, 2017.** © 2017 The Authors Magnetic Resonance in Medicine published by Wiley Periodicals, Inc. on behalf of International Society for Magnetic Resonance in Medicine. This is an open access article under the terms of the Creative Commons Attribution License, which permits use, distribution and reproduction in any medium, provided the original work is properly cited.

Key words: MRI; diffusion; IVIM; flow compensation; blood; perfusion

INTRODUCTION

"Blood is a juice of very special kind" (1) applies no less in the context of its MRI properties. One reason for its complex behavior is that its two main constituents, blood plasma (55%) and red blood cells (45%) (2), undergo exchange of water molecules (3,4). Not only have blood-relaxation times (5,6) and their dependence on oxygenation level been studied (7–9), but also the effects of diffusion were modeled and measured by Stanisz and Li (10,11). They took into account restricted diffusion in the red blood cells (RBCs), hindered diffusion in the plasma, and exchange between those compartments in a pulsed field gradient multi-spin-echo sequence (12) using short gradient pulses ($G_{max} = 6500$ mT/m). The use of short pulsed gradients enables the measurement of the average displacement propagator (13), and therefore can yield a good estimate of diffusion properties; however, on a typical clinical scanner ($G_{max} = 40$ mT/m), diffusion gradients are elongated to achieve a sufficiently strong weighting. In this case, application of the approach by Stanisz and Li (10,11) and derivation of an analytical expression is not straightforward.

Apart from staging hematomas (14), blood diffusion properties play an important role in intravoxel incoherent motion (IVIM) imaging (15), which allows one to separate the effects of blood motion and tissue water diffusion (16). In this framework, the diffusion-weighted signal attenuation caused by blood flow is modeled via a pseudo-diffusion coefficient D*, which is much larger than the self-diffusion coefficient D_b of blood. Although D_b is therefore negligible in typical IVIM experiments, this is not the case if flow-compensated (FC) diffusion gradients are used, which was first proposed by Ahn (17) and Maki (18). In a recent publication, the utility of using both monopolar (MP) and FC diffusion gradients for IVIM measurements in liver and pancreas was shown, which has the potential to measure characteristic length and velocity in vascular networks (19). The method presented here, however, used a fixed value of $D_b = 1.6\ \mu m^2$/ms, which was an estimate based on (10,11).

In this work, the apparent diffusion coefficient (ADC) of blood is characterized using a diffusion-weighted sequence on a clinical scanner. The multicompartment nature of blood is considered by varying the echo time (TE), diffusion time T, and diffusion gradient profile (FC or MP), and Monte Carlo simulations of blood diffusion are performed. Although the initial intent of this study was to provide an accurate estimate of D_b for FC IVIM (19), its results might also be relevant in the case of cardiac diffusion MRI (20,21), in which FC gradients are used, and add to the ongoing debate on the value of diffusion-weighted MRI in the assessment of intracranial hemorrhage (22).

METHODS

A phantom assembly was built holding rotatable sample tubes in a plastic frame within a water tank (Fig. 1a). Foam isolation was used to reduce cooling to less than 1°C during the 30-min MRI protocol, which was controlled using
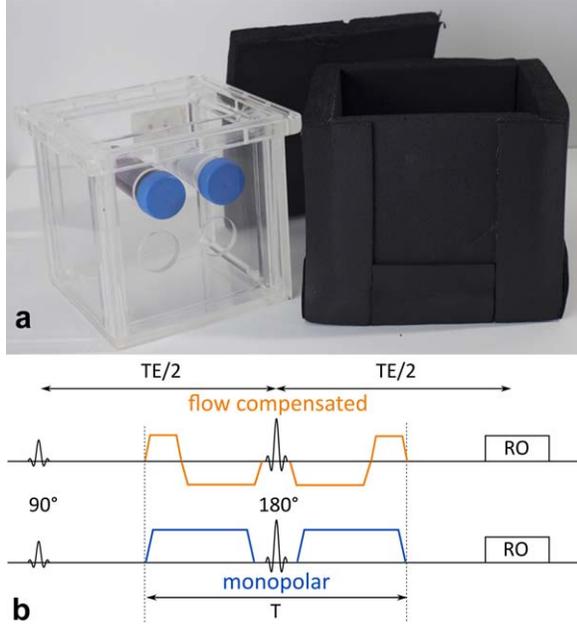
FIG. 1. **a**: Water tank with one blood sample and one water tube as a reference is placed inside foam insulation (right side). Sample tubes are manually rotatable around their long axis without the need to move the phantom between measurement steps. **b**: Sequence timing of the used diffusion MRI sequence with FC and MP gradient profiles. Diffusion time T can be varied independently of TE.

an analog thermometer. Blood was drawn from 10 consenting healthy volunteers (5 male, 5 female) via venipuncture of the forearm. Heparin was added (19 IU/mL), and blood was stored in a sample tube (60 mL) in a water bath at 37.5°C for up to an hour before it was measured. As depicted in Figure 1a, we always measured one blood sample simultaneously with one water-reference tube. For each blood sample, a blood count was obtained. The measurement protocol was divided into steps of less than 3-min duration, such that sample tubes could be rotated in between acquisitions to prevent sedimentation (8).

The phantom was placed inside a 12-channel head coil with sample tubes orientated parallel to $B_0 = 1.5$ T (Magnetom Symphony, Siemens Healthcare, Erlangen, Germany). An in-house-developed diffusion-weighted single-shot spin-echo echo-planar-imaging sequence was used, which allowed for setting the duration T of the diffusion-weighting block independently of TE (19). Both MP and FC diffusion gradients were implemented (Fig. 1b). The imaging parameters were as follows: field of view: 250×195 mm^2, nominal in-plane resolution: 2.5×2.5 mm^2, imaging matrix 100×78, slice thickness/gap: 5/2.5 mm, readout bandwidth: 2000 Hz/Px, repetition time = 2.5 s, partial Fourier: 0.75, Grappa 2. For each combination of T and TE, an unweighted scan was added before and after the diffusion-weighted scans, for which b-values 50 and 400 s/mm^2 were applied along the six directions (1,1,0), (1,0,1), (0,1,1), (−1,−1,0), (−1,0,−1), (0,−1,−1). First, T was varied between 40 and 100 ms (FC: 70 to 100 ms) in steps of 10 ms with fixed TE = 120 ms (T-dependence). Second, TE was varied between 60 and 200 ms with diffusion times fixed to the minimum time required to achieve b = 400 s/mm^2, which was $T_{min} = 40$ ms for MP and

$T_{min} = 70$ ms for FC (TE-dependence). Diffusion gradients were applied symmetrically around a refocusing pulse to minimize artifacts related to concomitant fields. For details on the implementation see (19). As highlighted by Stoeck et al, the gradient profile is second-order motion-compensated (23). An alternative implementation was demonstrated by Ahlgren et al. (24).

The ADC calculation was based on regions of interest and using all three b-values. Mean signal intensities were averaged over all diffusion-gradient directions and slices, as no dependence on the slice position was observed. A noise correction of the measured signal S_m according to $S_c = \sqrt{S_m^2 - 6\sigma^2}$ was performed, where σ is the average background noise of one of the six individually accessible receiver channels measured in the image outside the phantom. The ADC measurements, in which S_c was less than $\sqrt{60}\sigma$ in the b = 400 s/mm^2 image (equivalent to signal-to-noise ratio (SNR) $< \sqrt{10} \approx 3.2$) were excluded to avoid underestimation of the ADC. The factors 6 and $\sqrt{60}$ were derived for the sum-of-squares reconstruction based on the finding that the lower coil elements yield approximately half of the signal of the upper coil elements within the sample tubes, and assuming that each coil element can be corrected according to $\sqrt{S^2 - \sigma^2}$ (25) (for details see Supporting Text 1).

The Pearson product moment coefficient r was calculated for each combination of ADC with hematocrit (HCT), mean corpuscular volume (MCV), and hemoglobin concentration (HGB). Linear regression was performed in IGOR pro (WaveMetrics Inc, Portland, OR), if the null hypothesis of uncorrelated parameters was rejected at a significance level of 5% ($|r| > r_{crit}$). A paired two-sided t-test was used to compare MP and FC ADC values.

Monte Carlo simulations of blood diffusion were performed in MATLAB (R2015b, the MathWorks Inc, Natick, MA). Source code is available from https://github.com/awetscherek/bloodMC (SHA1: xxx). The RBC shape was modeled by oblate cylinders of 8.00 μm diameter and height of 1.75 μm, which were scaled to match the sample MCV. The RBC was placed centered in a cuboid unit cell, sized such that HCT equaled RBC volume fraction. The resulting surface-to-volume ratio is 1.64 μm^{-1}, which is close to the typical surface-to-volume ratio of 1.5 μm^{-1} for red blood cells reported by Linderkamp (26). Diffusion in plasma was governed by $D_p = 2.75 \cdot 10^{-3}$ mm^2/s, as reported for 37°C (10), and by $D_e = 1.00 \cdot 10^{-3}$ mm^2/s in erythrocytes. With free-water concentrations of $c_p = 0.95$ and $c_e = 0.70$, the fraction of blood water contained in RBCs is given by f $= c_e \cdot$ HCT$/[c_e \cdot$ HCT $+ c_p \cdot$ (1 - HCT)] (6). The probability for transmission from compartment i is modeled as $P = 2 d_s \kappa_i/D_i$ following (27), where d_s is the distance to the membrane. We chose a pre-exchange lifetime of $\tau_e = 12$ ms based on the range reported in literature for water molecules in RBCs (28), yielding the membrane permeability $\kappa_e = (V/S)/\tau_e$ with the surface-to-volume ratio of the RBCs. For stable concentrations, $\kappa_e = \kappa_p \cdot (c_p/c_e)$ follows.

A total of 300,000 particle trajectories $\boldsymbol{x}(t)$ were simulated for a duration of TE = 120 ms, and trajectory center of mass location $\boldsymbol{x}_{cm,k} = \frac{1}{\Delta t_k} \int_{t_{k-1}}^{t_k} \boldsymbol{x}(t) dt$ was saved for each of the K time intervals $\Delta t_k = t_k - t_{k-1}$ of constant diffusion
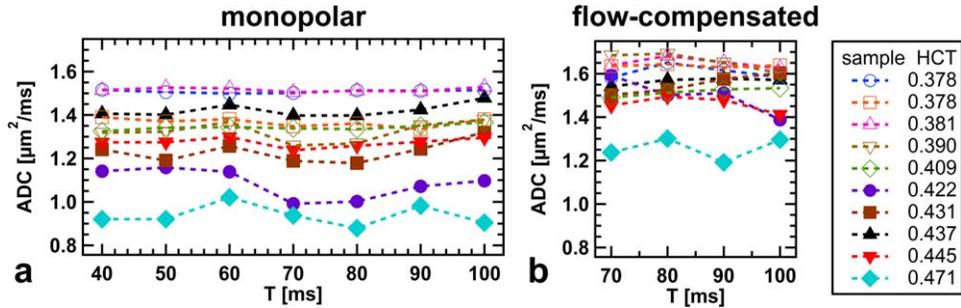
FIG. 2. No characteristic dependence of measured ADC on diffusion time T is visible in the blood samples. Blood ADCs are larger for FC gradients (**b**) than for MP gradients (**a**). Samples with lower HCT exhibit a tendency toward higher ADC. The ADCs concurrently measured in water samples are provided as Supporting Figure S1.

gradient. Gradients are switched on at t_0 and off at t_K with gradient sign switching at t_k with $0 < k < K$. For the sequence in use, those time points are given by $t_k = TE/2 + (k-1) \cdot T/2$ for the MP ($k \in 0,1,2$) and $t_k = TE/2 + T/4 \cdot \mathrm{sgn}(k-2) \cdot \sqrt{2}^{|k-2|}$ for the FC profile ($k \in 0,1,2,3,4$), as described in (19). The effective gradient profiles used in the simulations are visualized in Supporting Figures S1a (MP) and S1b (FC). Step size was chosen as 1% of the shortest dimension (distance between neighboring RBCs). For example, in the case of HCT = 43% and MCV = 87.7 fL, this results in a step size of 8.56 nm, resulting in a total of $2.7 \cdot 10^7$ steps for TE = 120 ms. The runtime ranged from 5.5 to 12.5 h on an Intel Xeon E5-1660 v3 with 128 GB memory. Distributions of accumulated phase φ were obtained by weighting $\mathbf{x}_{cm}$ along 10000 diffusion gradient directions $\mathbf{g}$ for isotropic weighting, where the magnitude of $\mathbf{g}$ corresponded to b = 400 s/mm^2:

$$\varphi = \varphi'\sqrt{b} = \gamma\mathbf{g} \cdot \sum_{k=1}^{K} \Delta t_k \mathbf{x}_{cm,k}(-1)^k \qquad [1]$$

This connection between φ and $\mathbf{x}_{cm,k}$ goes back to (29). Recognizing that φ is proportional to $|\mathbf{g}|$, and thus $\sqrt{b}$, allows one to introduce a normalized phase φ', similar to the concept used in (19). From the results of the Monte Carlo simulations, the distribution of normalized phases φ' can be obtained for each combination of gradient profile and diffusion time. From those one can calculate $\mathrm{ADC}_b = -\frac{1}{b}\ln|\langle e^{i\varphi'\sqrt{b}}\rangle|$, which is the ADC value that one would obtain from one measurement at b and one without diffusion weighting (b = 0).We also calculated excess diffusional kurtosis (30) $K_{app} = \langle\varphi'^4\rangle/(\langle\varphi'^2\rangle)^2 - 3$ and the limit of ADC_b for small b-values, $\mathrm{ADC}_0 := \lim_{b\to 0}\mathrm{ADC}_b = \langle\varphi'^2\rangle/2$, which is equivalent to the Gaussian phase approximation as shown elsewhere (19). According to Equation [36] in (30), those properties are linked as follows:

$$ADC_b = -\frac{1}{b}\ln\frac{S(b)}{S(0)} = ADC_0 - \frac{b}{6}ADC_0^2 K_{app} + O(b^2) \qquad [2]$$

RESULTS

Measured ADCs are plotted against diffusion time T in Figure 2 for blood samples (Figs. 2a and 2b). Data from simultaneously acquired water reference tubes are provided as Supporting Figures S1c and S1d. Monopolar ADCs are

displayed on the left (Fig. 2a), whereas FC ADCs are displayed on the right (Fig. 2b). Different markers and colors are used to distinguish blood samples (HCT is displayed in the legend), where unfilled markers depict samples from female volunteers. Errors for individual ADC measurements based on the analysis of 95% confidence intervals were in the range of $\pm(0.03$–$0.07)$ µm^2/ms for MP gradients and in the range of $\pm(0.06$–$0.11)$ µm^2/ms for FC measurements, in which samples with faster T_2 relaxation exhibit lower SNR, resulting in higher variance.

Although ADCs measured in the water reference agree within error margins across all measurements and are in accordance with literature (31), blood ADCs from different samples differ strongly for both MP and FC diffusion gradients. Because the uncertainty in temperature adjustment is only of the order of 1°C, ADC differences between blood samples must be attributed to different blood composition. Flow-compensated diffusion weighting yields higher ADC values compared with MP gradients for blood ($P < 10^{-14}$), whereas ADCs measured in the water reference are independent of the gradient profile ($P = 0.083$). Considering all measurements, no characteristic dependence of the ADC on T is apparent.

Hematocrit, MCV, and HGB Dependence

For each sample, ADCs averaged over all diffusion times were plotted in Figure 3 against HCT, MCV, and HGB. Results from measurements with FC and MP diffusion encoding are depicted by different markers and colors. Because statistical analysis indicated a correlation between ADC and HCT (FC: r = −0.82, $P = 0.007$; MP: r = −0.56, $P = 0.11$), linear regression was performed yielding ADC_{FC}[µm^2/ms] = 1.545 + (0.42 − HCT) · 2.169 and ADC_{MP}[µm^2/ms] = 1.307 + (0.42 − HCT) · 2.846. No ADC dependence on MCV becomes apparent (FC: r = 0.18, $P = 0.64$ and MP: r = 0.40, $P = 0.28$), whereas ADC versus HGB shows a trend similar to the relation between ADC and HCT (FC: r = −0.76, $P = 0.017$ and MP: r = −0.66, $P = 0.055$): ADC_{FC}[µm^2/ms] = 1.551 + (14.5 − HGB[g/dL]) · 0.053 and ADC_{MP}[µm^2/ms] = 1.312 + (14.5 - HGB[g/dL]) · 0.087.

Echo Time Dependence

Figure 4 shows the result of the second measurement series, for which the echo time was varied, whereas the diffusion time was fixed. Individual samples are marked as in Figure 2. Using the unweighted (b = 0 s/mm^2) measurements from
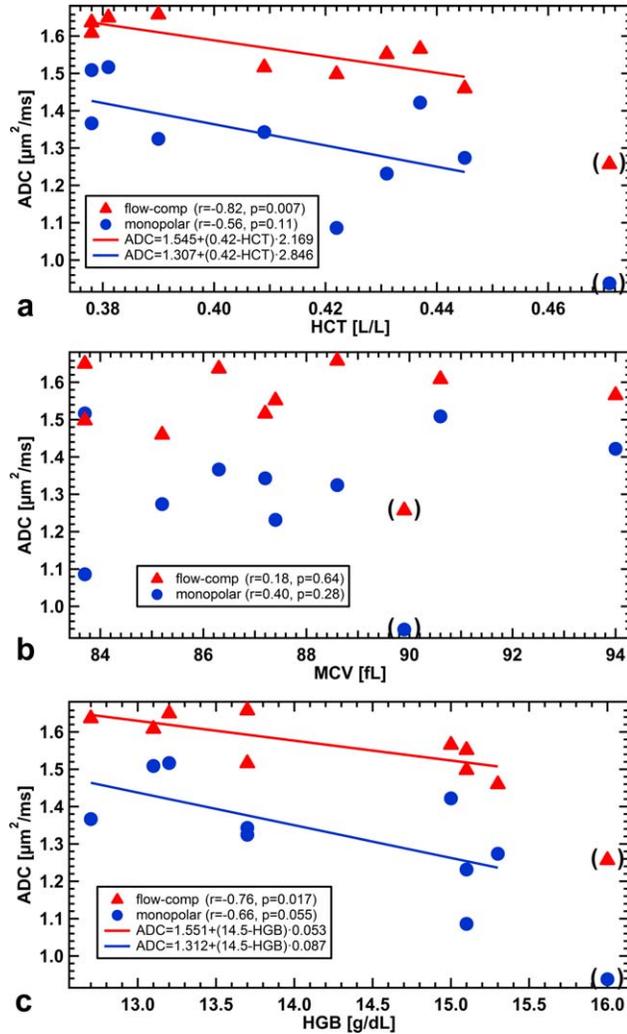
FIG. 3. ADCs averaged over all diffusion times versus hematocrit (**a**), mean cell volume (**b**), and hemoglobin concentration (**c**) for FC and MP diffusion gradients. Linear regression was performed, where $|r| > r_{crit} = 0.666$. Although ADCs decrease for increasing HCT and HGB (significant only for FC gradients), no trend is apparent for MCV. Flow-compensated diffusion gradients yield larger ADCs. Data points in parentheses suffered from very low SNR and were excluded from the analysis (see also Fig. 4).

range present in our blood samples (denoted by different colors; see Figs. 5c and 5d). The MCV was set to the mean value of the experimental blood samples, which was 87.7 fL. $ADC_0 = \langle \varphi^2/2 \rangle / b$ (assuming Gaussian phase distribution) was calculated and shows no T dependence for MP gradients (continuous lines in Fig. 5a), whereas a decreasing ADC_0 is found for FC gradients (dashed lines in Fig. 5b), which approaches the values of Figure 5a for longer diffusion times. Excess diffusional kurtosis is a measure of the deviation of the phase distribution from a Gaussian function, and decreases for both gradient profiles at larger T (Figs. 5c and 5d). It is directly related to the measured ADC_b according to Equation [2], explaining
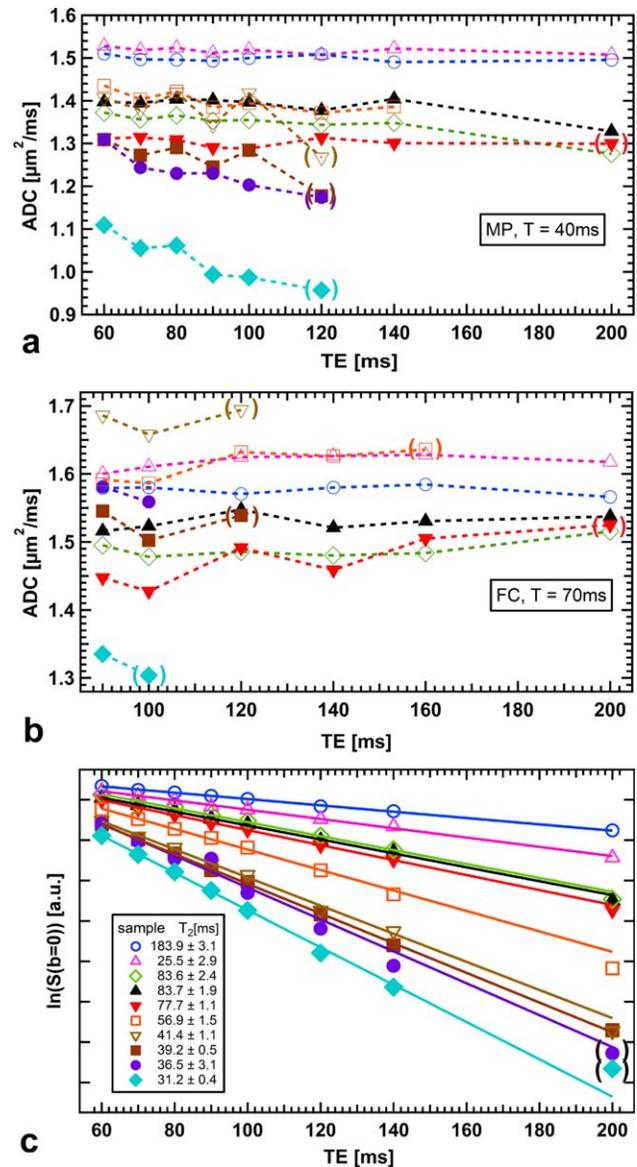
FIG. 4. Blood ADC versus echo time for MP (**a**) and FC (**b**) diffusion weighting. Sample markers and colors equal those in Figure 2. Data points in parenthesis are based on measurements with low SNR (< 5). Although ADCs do not exhibit clear TE dependence for samples with $T_2 > 50$ ms, ADCs decrease with TE for $T_2 < 40$ ms in the MP case. **c**: Logarithmic unweighted signal intensity versus echo time. Mono-exponential fits were used to estimate T_2.

this series, T_2 relaxation times were calculated (Fig. 4c). Because of the short T_2 relaxation time of some samples, the SNR of the diffusion weighted image at longer TE is not sufficient to provide reliable ADC measurements for those samples. In Figures 4a and 4b, only data points in which the signal at $b = 400$ s/mm^2 fulfilled the SNR criterion (SNR > 3.2) are displayed, and those with $3.2 < SNR < 5$ are marked with parentheses. The two samples with the shortest T_2 relaxation times were found to show a significant decrease ($P = 0.014$ and 0.028) of the ADC with TE (Fig. 4a), whereas samples with longer T_2 relaxation time were not found to exhibit a particular TE dependence.

Simulation

Figure 5 shows the results of the simulations, which were performed for different HCT values over the HCT

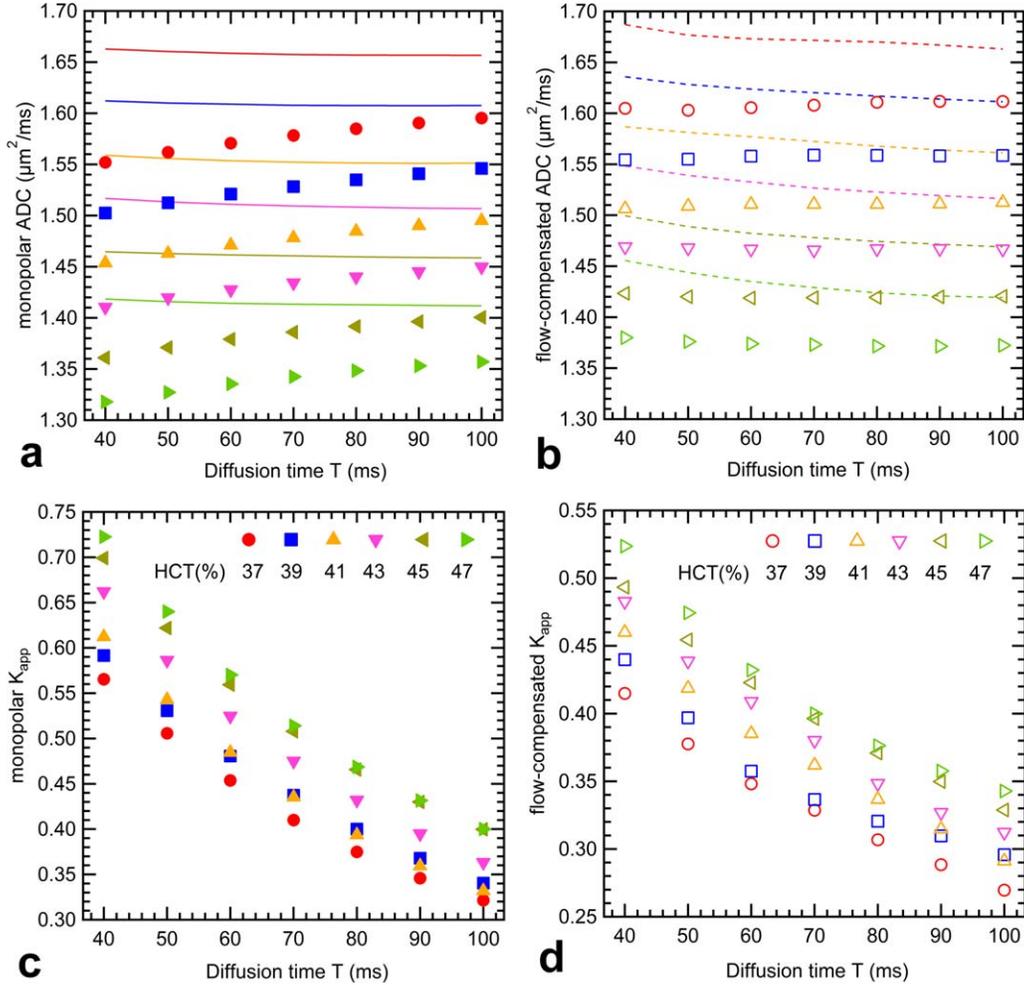FIG. 5. Simulation results for MP (**a, c**) and FC (**b, d**) gradients for different diffusion times and fixed TE = 120 ms. Hematocrit is the only differing parameter, and assignment of color is shown in (**c**) and (**d**). ADC_0 is denoted by lines and does not show a T dependence in the MP case (**a**), whereas ADC_0 decreases with T in the FC case (**b**). $K_{app} > 0$ indicates non-Gaussian diffusion (**c, d**) and decreases with T, which is reflected in the T dependence of ADC_{400} (**a**). Effects balance out in the FC case (**b**).

the smaller values of ADC_{400} (markers in Figs. 5a and 5b), when compared with ADC_0.

The simulation confirms the experimental findings (Fig. 2) that the measured ADC exhibits a strong dependence on HCT. It should be noted, however, that the range of ADC_{400} values in the simulation (Figs. 5a and 5b) is smaller (1.33–1.58 μm^2/ms) than in the experiment (0.9–1.65 μm^2/ms), which presumably reflects that the simplified model is only a rough approximation of the real situation.

DISCUSSION

Diffusion-weighted imaging was performed on blood samples of 10 healthy volunteers using a phantom and measurement protocol devised to minimize the effects of sedimentation (8) and cooling. A water-reference sample was acquired simultaneously, and the ADC measured in water did not exhibit any dependence on diffusion time, TE, or on the applied diffusion gradient profile, which

ensured that applied b-values were correct for the in-house-developed MRI sequence (19).

The finding that ADCs measured with FC gradients were higher than those obtained from MP gradients can be explained by two effects. First, in the concept of "effective diffusion time" T_{eff}, the FC profile can be understood as three oscillations of the bipolar profile, resulting in $T_{eff,FC} \approx T_{eff,MP}/3$. A measurement with shorter T_{eff} is less sensitive to diffusion restriction by the RBC membrane and thus exhibits a higher ADC_0 (32), which is confirmed by our simulations (Figs. 5a and 5b). The second effect is related to diffusional kurtosis, which causes a reduction of measured ADC_b compared with ADC_0. Our simulations reveal that K_{app} is higher for MP gradients (Fig. 5c) than for FC gradients (Fig. 5d), further increasing the difference in ADC_{400} between FC and MP gradients (Figs. 5a and 5b). Similar results were found by Portnoy et al. (33), who speculated that the different kurtosis found for (non-FC) pulsed-gradient spin-echo and (FC) oscillating-gradient spin-echo pulse sequences originated from the different gradient spectrum $F(\omega)$. The dependence of the kurtosis

on T found in Figures 5c and 5d could be related to exchange between the compartments, which was found by Jensen and Helpern (34).

Although the used b-value of 400 s/mm^2 is rather low compared with the optimal b-value of b = 1.278/ADC that one would choose in the case of a mono-exponential decay (35,36), the influence of the kurtosis term is not negligible; it can be understood from Figure 5b that the two T dependencies from restriction and exchange balance out for our choice of simulation parameters. The increase in ADC$_{400}$ between T = 40 ms and T = 100 ms predicted by the simulations in Figure 5a is less than 0.05 μm^2/ms, which is of the order of our measurement uncertainty, explaining why it was not revealed by our experimental data. A characterization with substantially increased SNR, such as at higher field strength, would be necessary to experimentally resolve a possible T dependence of the blood ADC. An experimental characterization of the diffusional kurtosis would have made our work more complete, but the necessary measurements at high b-values with the used FC gradient profile could only be achieved with high-performance gradient coils.

Although our experimental results would indicate that there is a correlation between HCT/HGB and blood ADC, it is only significant for FC gradients in this study. It is backed up by the simulations, which also show a strong dependence of ADC on HCT values, but the range of ADC values is not as large as in the experiment. In preparatory simulations, we found that this range and difference in ADC between MP and FC gradients depend heavily on the chosen membrane permeability. For the simulations presented here, we chose to stick to a literature value of τ_e = 12 ms based on (28), which was in better agreement with our experimental data than the range of τ_e = 6–9 ms reported in (37). Choosing an even longer intracellular pre-exchange lifetime than τ_e = 12 ms for the simulations (corresponding to a lower membrane permeability) would have matched our experimental data better. This could be related to the approximation of the biconcave disc shape by a cylinder (changing the surface-to-volume ratio and thus membrane permeability κ_e) or to membrane degradation after blood was taken. Despite frequent mixing, orientation of the erythrocytes in the static magnetic field might have played a role (38).

One limitation of our study is that blood oxygenation was not recorded. Blood oxygenation is well known to influence T$_2$ (39–41), with lower oxygen saturation resulting in shorter relaxation times as a result of magnetic field gradients caused by susceptibility differences between RBCs and plasma (8). This is the basis for blood-oxygenation-level dependent (BOLD) contrast imaging (42). A further study measuring blood diffusion with monitoring of the blood oxygenation level would be needed to separate the effects of HCT/HGB and those originating from changes in blood oxygenation on the whole-blood ADC. Relaxation time effects and additional gradients caused by susceptibility mismatch could be incorporated into the Monte-Carlo simulations, which might affect the simulation results of the ADC dependence on T (Figs. 5a and 5b), but could also give insight into the dependence of the ADC on TE, which we experimentally observed in some samples (Figs. 4a and 4b).

Although we tried to exclude low SNR as a cause, the decline in ADC remains significant for the two samples with the fastest T$_2$ relaxation when limiting our analysis to data with SNR greater than 5. A TE dependence of the blood ADC could only be explained by different relaxation times and diffusivities in plasma and RBCs. Although those conditions are fulfilled, the system is in the fast exchange limit for relaxation, thus exhibiting only a mono-exponential T$_2$ relaxation (Fig. 4c) and suppressing a TE dependence of the ADC. A possible explanation for the observed TE dependence in the samples with the fastest T$_2$ relaxation could thus be membrane degradation and reduced exchange as a consequence of the presumably lower oxygen saturation. This theory, however, could only be proven in a study in which oxygen saturation of the blood samples was measured.

Another limitation is that blood composition differs between different types of blood vessels. Apart from changes in oxygen and carbon dioxide concentrations, hematocrit (43) and erythrocyte volume (44) differ between blood in veins and capillaries, which will affect the ADC. As the characteristic length scales obtained with FC IVIM (19) would indicate, the IVIM effect is caused primarily by blood flow in arterioles and venules, with the latter containing 4 times more blood volume (45). Assuming that blood constitution in veins and venules is similar, our results should be applicable for IVIM.

In conclusion, we found no dependence of the ADC on diffusion time T in the range of 40 to 100 ms. The ADCs measured with FC gradients were larger than those obtained with MP encoding. Large ADC differences between samples were found, correlating with HCT and HGB. For accuracy of FC IVIM measurements, we recommend the use of a blood ADC of 1.54 ± 0.12 μm^2/ms for FC encoding and 1.30 ± 0.18 μm^2/ms for MP encoding. If a blood count is available, we recommend the use of ADC$_{MP}[\mu m^2/ms] = 1.307 + (0.42 - HCT) \cdot 2.846$ and ADC$_{FC}[\mu m^2/ms] = 1.545 + (0.42 - HCT) \cdot 2.169$, respectively.

REFERENCES

1. von Goethe JW. Faust. Eine Tragödie. Tübingen, Germany: Cotta; 1808.
2. McGeown JG. Blood and related physiology. In: Master medicine: physiology, 3rd ed. London: Churchill Livingstone; 2007.
3. Fabry ME, Eisenstadt M. Water exchange between red cells and plasma. Measurement by nuclear magnetic relaxation. Biophys J 1975;15:1101–1110.
4. Andrasko J. Water diffusion permeability of human erythrocytes studied by a pulsed gradient NMR technique. Biochim Biophys Acta 1976;428:304–311.
5. Barth M, Moser E. Proton NMR relaxation times of human blood samples at 1.5 T and implications for functional MRI. Cell Mol Biol (Noisy-le-grand) 1997;43:783–791.
6. Li W, Grgac K, Huang A, Yadav N, Qin Q, van Zijl PC. Quantitative theory for the longitudinal relaxation time of blood water. Magn Reson Med 2016;76:270–281.
7. Li DB, Waight DJ, Wang Y. In vivo correlation between blood T_2^* and oxygen saturation. J Magn Reson Imaging 1998;8:1236–1239.
8. Spees WM, Yablonskiy DA, Oswood MC, Ackerman JJ. Water proton MR properties of human blood at 1.5 Tesla: magnetic susceptibility, T_1, T_2, T_2^*, and non-Lorentzian signal behavior. Magn Reson Med 2001;45:533–542.
9. Ogawa S, Lee TM. Magnetic resonance imaging of blood vessels at high fields: in vivo and in vitro measurements and image simulation. Magn Reson Med 1990;16:9–18.
10. Stanisz GJ, Li JG, Wright GA, Henkelman RM. Water dynamics in human blood via combined measurements of T$_2$ relaxation and

diffusion in the presence of gadolinium. Magn Reson Med 1998;39: 223–233.

11. Li JG, Stanisz GJ, Henkelman RM. Integrated analysis of diffusion and relaxation of water in blood. Magn Reson Med 1998;40:79–88.

12. van Dusschoten D, Moonen CT, de Jager PA, Van As H. Unraveling diffusion constants in biological tissue by combining Carr-Purcell-Meiboom-Gill imaging and pulsed field gradient NMR. Magn Reson Med 1996;36:907–913.

13. Kärger J, Heink W. The propagator representation of molecular transport in microporous crystallites. J Magn Reson 1983;51:1–7.

14. Atlas SW, DuBois P, Singer MB, Lu D. Diffusion measurements in intracranial hematomas: implications for MR imaging of acute stroke. AJNR Am J Neuroradiol 2000;21:1190–1194.

15. Le Bihan D, Breton E, Lallemand D, Grenier P, Cabanis E, Laval-Jeantet M. MR imaging of intravoxel incoherent motions: application to diffusion and perfusion in neurologic disorders. Radiology 1986; 161:401–407.

16. Le Bihan D, Breton E, Lallemand D, Aubin M-L, Vignaud J, Laval-Jeantet M. Separation of diffusion and perfusion in intravoxel incoherent motion MR imaging. Radiology 1988;168:497–505.

17. Ahn CB, Lee SY, Nalcioglu O, Cho ZH. The effects of random directional distributed flow in nuclear magnetic resonance imaging. Med Phys 1987;14:43–48.

18. Maki JH, MacFall JR, Johnson GA. The use of gradient flow compensation to separate diffusion and microcirculatory flow in MRI. Magn Reson Med 1991;17:95–107.

19. Wetscherek A, Stieltjes B, Laun FB. Flow-compensated intravoxel incoherent motion diffusion imaging. Magn Reson Med 2015;74:410–419.

20. Gamper U, Boesiger P, Kozerke S. Diffusion imaging of the in vivo heart using spin echoes-considerations on bulk motion sensitivity. Magn Reson Med 2007;57:331–337.

21. Froeling M, Strijkers GJ, Nederveen AJ, Chamuleau SA, Luijten PR. Diffusion tensor MRI of the heart—in vivo imaging of myocardial fiber architecture. Curr Cardiovasc Imaging Rep 2014;7:9276.

22. Whang JS, Kolber M, Powell DK, Libfeld E. Diffusion-weighted signal patterns of intracranial haemorrhage. Clin Radiol 2015;70:909–916.

23. Stoeck CT, von Deuster C, Genet M, Atkinson D, Kozerke S. Second-order motion-compensated spin echo diffusion tensor imaging of the human heart. Magn Reson Med 2016;75:1669–1676.

24. Ahlgren A, Knutsson L, Wirestam R, Nilsson M, Ståhlberg F, Topgaard D, Lasič S. Quantification of microcirculatory parameters by joint analysis of flow-compensated and non-flow-compensated intravoxel incoherent motion (IVIM) data. NMR Biomed 2016;29:640–649.

25. Gudbjartsson H, Patz S. The Rician distribution of noisy MRI data. Magn Reson Med 1995;34:910–914.

26. Linderkamp O, Wu PY, Meiselman HJ. Geometry of neonatal and adult red blood cells. Pediatr Res 1983;17:250–253.

27. Fieremans E, Novikov DS, Jensen JH, Helpern JA. Monte Carlo study of a two-compartment exchange model of diffusion. NMR Biomed 2010;23:711–724.

28. Bruno E, Digilio G, Cabella C, de Reggi A, Baroni S, Mainero V, Aime S. Water exchange across the erythrocyte plasma membrane studied by HR-MAS NMR spectroscopy. Magn Reson Med 2006;56:978–985.

29. Mitra PP, Halperin BI. Effects of finite gradient-pulse widths in pulsed-field-gradient diffusion measurements. J Magn Reson A 1995; 113:94–101.

30. Jensen JH, Helpern JA, Ramani A, Lu HZ, Kaczynski K. Diffusional kurtosis imaging: the quantification of non-Gaussian water diffusion by means of magnetic resonance imaging. Magn Reson Med 2005;53: 1432–1440.

31. Holz M, Heil SR, Sacco A. Temperature-dependent self-diffusion coefficients of water and six selected molecular liquids for calibration in accurate ^{1}H NMR PFG measurements. Phys Chem Chem Phys 2000;2:4740–4742.

32. Gore JC, Xu JZ, Colvin DC, Yankeelov TE, Parsons EC, Does MD. Characterization of tissue structure at varying length scales using temporal diffusion spectroscopy. NMR Biomed 2010;23:745–756.

33. Portnoy S, Flint JJ, Blackband SJ, Stanisz GJ. Oscillating and pulsed gradient diffusion magnetic resonance microscopy over an extended b-value range: implications for the characterization of tissue microstructure. Magn Reson Med 2013;69:1131–1145.

34. Jensen JH, Helpern JA. MRI quantification of non-Gaussian water diffusion by kurtosis analysis. NMR Biomed 2010;23:698–710.

35. Gabr RE, El-Sharkawy A-MM, Schär M, Weiss RG, Bottomley PA. High-energy phosphate transfer in human muscle: diffusion of phosphocreatine. Am J Physiol Cell Physiol 2011;301:C234–C241.

36. Fleysher R, Fleysher L, Gonen O. The optimal MR acquisition strategy for exponential decay constants estimation. Magn Reson Imaging 2008;26:433–435.

37. Quirk JD, Bretthorst GL, Duong TQ, Snyder AZ, Springer CS, Jr., Ackerman JJ, Neil JJ. Equilibrium water exchange between the intra- and extracellular spaces of mammalian brain. Magn Reson Med 2003; 50:493–499.

38. Higashi T, Yamagishi A, Takeuchi T, Kawaguchi N, Sagawa S, Onishi S, Date M. Orientation of erythrocytes in a strong static magnetic field. Blood 1993;82:1328–1334.

39. Thulborn KR, Waterton JC, Matthews PM, Radda GK. Oxygenation dependence of the transverse relaxation time of water protons in whole blood at high field. Biochim Biophys Acta 1982;714:265–270.

40. Chen JJ, Pike GB. Human whole blood T_2 relaxometry at 3 Tesla. Magn Reson Med 2009;61:249–254.

41. Stefanovic B, Pike GB. Human whole-blood relaxometry at 1.5T: assessment of diffusion and exchange models. Magn Reson Med 2004;52:716–723.

42. Ogawa S, Lee TM, Nayak AS, Glynn P. Oxygenation-sensitive contrast in magnetic resonance image of rodent brain at high magnetic fields. Magn Reson Med 1990;14:68–78.

43. Perkkiö J, Keskinen R. Hematocrit reduction in bifurcations due to plasma skimming. Bull Math Biol 1983;45:41–50.

44. Carr RT, Wickham LL. Influence of vessel diameter on red cell distribution at microvascular bifurcations. Microvasc Res 1991;41:184–196.

45. Henkelman RM, Neil JJ, Xiang Q-S. A quantitative interpretation of IVIM measurements of vascular perfusion in the rat brain. Magn Reson Med 1994;32:464–469.

SUPPORTING INFORMATION

Additional Supporting Information may be found in the online version of this article.

Text 1. Derivation of factors for noise correction and low SNR data exclusion criterion.

Fig. S1. a, b: Effective diffusion-weighting profiles used for the Monte Carlo simulations, which correspond to the diffusion sequence displayed in Figure 1b. To obtain a particular b-value, the waveforms have to be scaled by the gradient amplitude g such that $b=a\gamma^2 g^2 T^3$ with $a=1/12$ for the MP profile (**a**) and $a=\sqrt{2}/8-1/6$ in the FC case (**b**). **c, d**: ADCs measured in a water-reference tube simultaneously with the blood samples (same marker as the respective samples in Fig. 2). Water ADCs agree within 3% error across all measurements and with literature values.